

pubs.acs.org/crystal Article

Crystal Growth and Phase Formation of High-Entropy Rare-Earth Aluminum Perovskites

Matheus Pianassola,* Bryan C. Chakoumakos, Charles L. Melcher, and Mariya Zhuravleva



Cite This: https://doi.org/10.1021/acs.cgd.2c01130



Read Online

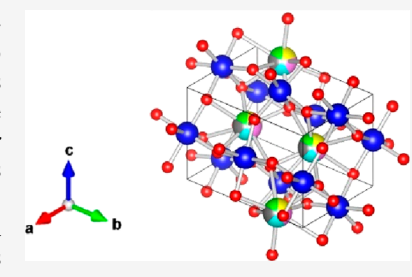
ACCESS I

III Metrics & More

Article Recommendations

SI Supporting Information

ABSTRACT: We demonstrate for the first time the crystal growth of high-entropy rare-earth (RE) aluminum perovskites (REAlO₃) using the micro-pulling-down method to inform future exploration of functional crystals. To determine how composition affects phase formation, we formulate equiatomic compositions containing five REs from the following list: Lu, Yb, Tm, Er, Y, Ho, Dy, Tb, Gd, Eu, Sm, Nd, Pr, Ce, La. To test whether combinations of REs with similar ionic radii may favor a single phase, compositions containing REs with consecutive or nonconsecutive ionic radius values were formulated. Powder and single-crystal X-ray diffraction indicate that crystals containing only REs with similar ionic radii that form orthorhombic single-RE REAlO₃ are a single phase. Crystals containing REs with dissimilar ionic radii or mixtures of REs that form orthorhombic,



rhombohedral, and tetragonal single-RE REAlO $_3$ are a mixture of phases. The elemental distribution in single-phase crystals analyzed via electron probe microanalysis confirms no evidence of preferential incorporation of any of the constituent REs. The distribution and composition of secondary phases were analyzed via scanning electron microscopy and energy dispersive spectroscopy; secondary phases were seen as a small region in the center of the crystals with branching features closer to the outer surface.

1. INTRODUCTION

Pioneering reports on bulk high-entropy oxide single crystals have motivated further studies on the growth of complex crystals from various compositional systems. 1–3 The interest in such crystals originates from the enhanced properties seen in polycrystalline high-entropy oxides, such as reversible energy storage, low thermal conductivity for environmental barriers, and high thermal stability. In those oxides, admixing five or more cations in equiatomic amounts leads to an entropy-driven phase stabilization and a synergistic effect on functional properties. Demonstrations of the growth of highly complex oxide crystals have been limited to a few rare-earth-based compositional systems including aluminum garnets, 1,6,7 titanates, 2,8 borates, 3,9 calcium borates, 10,11 and sesquioxides. The practical aspect of the growth of crystals from other highentropy compositional systems remains unexplored.

The field of crystal growth of high-entropy rare-earth (RE) aluminates attracts attention due to the possibility of maximizing the luminescence properties of analogous low-entropy crystals. Single-RE aluminum garnet (RE₃Al₅O₁₂) and perovskite (REAlO₃) crystals formed by Lu, Y, and Gd are commercially used for scintillation and lasing applications. ^{13–16} Several studies have proven that the performance of garnet crystals can be improved by admixing two or three REs. ^{17–20} This motivated studies on the practical aspect of crystal growth of high-entropy garnets. ^{1,6} Similar admixing studies on aluminum perovskites are limited^{21–25} and high-entropy perovskites have been only produced as polycrystalline ceramics. ²⁶ Therefore, this study aims to demonstrate the

growth of complex perovskites and leverage the future development of functional, complex perovskite crystals.

The correlation between the RE3+ ionic radius and the crystal structure of REAlO3 compounds is summarized in Table 1. Here, Y is referred to as a RE element for simplicity. An orthorhombic, rhombohedral, or tetragonal structure can be assumed by REAlO₃ compounds and their unit cells are shown in Figure 1. Smaller cations from Lu³⁺ to Sm³⁺ form an orthorhombic REAlO3 structure with Pnma space group where RE³⁺ have an 8-fold square antiprismatic coordination and Al³⁺ have a 6-fold slightly distorted octahedral coordination toward O²⁻²⁷⁻²⁹ Such REAlO₃ are often reported with the Pbnm space group, which is equivalent to the Pnma space group and is described by a permutation of its a, b, c axes. The larger Nd3+, Pr3+, and La3+ form a rhombohedral REAlO3 structure with $R\overline{3}ch$ space group where RE³⁺ has a 12-fold cuboctahedral coordination and Al3+ has a 6-fold octahedral coordination toward O^{2-.34} Although Ce³⁺ has an ionic radius similar to that of Pr3+ and La3+, CeAlO3 has a tetragonal structure with P4/ mmm space group where RE3+ has a 12-fold cuboctahedral coordination and Al3+ has a 6-fold octahedral coordination toward O^{2-.35} In CeAlO₃, the site occupancy factor for O²⁻

Received: October 6, 2022 Revised: November 28, 2022



Table 1. List of RE³⁺ Cations Ordered from Small to Large Ionic Radius³⁷ and Crystal Structure²⁷ of the Respective Single-RE REAlO₃ Compounds

RE ³⁺ cation	RE ³⁺ ionic radius for CN VI (Å)34	REAlO ₃ unit cell geometry and space group
Lu ³⁺	0.848	orthorhombic (Pnma)
Yb^{3+}	0.858	orthorhombic (Pnma)
Tm^{3+}	0.869	orthorhombic (Pnma)
Er^{3+}	0.881	orthorhombic (Pnma)
Y^{3+}	0.892	orthorhombic (Pnma)
Ho^{3+}	0.894	orthorhombic (Pnma)
Dy^{3+}	0.908	orthorhombic (Pnma)
$\mathrm{Tb^{3+}}$	0.923	orthorhombic (Pnma)
Gd^{3+}	0.938	orthorhombic (Pnma)
Eu^{3+}	0.950	orthorhombic (Pnma)
Sm^{3+}	0.964	orthorhombic (Pnma)
Nd^{3+}	0.995	rhombohedral $(R\overline{3}c)$
Pr^{3+}	1.013	rhombohedral $(R\overline{3}c)$
Ce ³⁺	1.034	tetragonal (P4/mmm)
La ³⁺	1.061	rhombohedral $(R\overline{3}c)$

sitting at 2f Wyckoff sites is 0.5, which is represented by half-filled spheres in the P4/mmm unit cell in the tetragonal unit cell in Figure 1.

In this work, we demonstrate the crystal growth of highentropy RE aluminum perovskites and correlate their composition and phase formation. We focus on seven REAlO $_3$ compositions containing five REs in equiatomic amounts to fractionally occupy the rare-earth cation sublattice. Our composition formulation is based on the premise that REs with similar ionic radii may favor the formation of single-phase high-entropy oxides. Compositions containing REs with consecutive or nonconsecutive ionic radius values were formulated to test that premise. Crystals were grown via directional solidification by the micropulling-down (mPD) method. This growth technique is optimal for materials development due to the small amount of material needed (\sim 1 g) and the fast pulling rates that can be achieved (up to 20 mm/min).

2. METHODS

2.1. Composition Formulation. High-entropy REAlO₃ compounds were formulated with five REs mixed in equiatomic amounts to study how phase formation is affected by two composition parameters: (1) the similarity in their ionic radii and (2) the type of REs in terms of the structure of the respective single-RE REAlO₃. Table 2 is a list of the compositions studied with the respective ID,

the number of REs that form each of the three structures observed in single-RE REAlO₃, and the average ionic radius (AIR). Previous work demonstrated that REs with similar ionic radii may favor the formation of a single phase in high-entropy oxides.³⁶ To test that concept and study the effect of the similarity of the RE³⁺ ionic radii on phase formation, compositions A, B, D, and E have only REs with consecutive ionic radius values in Table 1, while compositions C, F, and G have REs with nonconsecutive ionic radius values. To study the effect of the type of REs on phase formation, compositions A–D have only REs that form orthorhombic single-RE REAlO₃, while compositions E–G have mixtures of REs that form an orthorhombic, rhombohedral, and tetragonal single-RE REAlO₃.

2.2. Crystal Growth. Cylindrical Ø3 mm crystals were grown by the mPD method³⁸ using a KDN Dai-Ichi Kiden furnace with an RF generator model TR-02001 operated at 26 kVA. The starting powders were Lu₂O₃, Yb₂O₃, Tm₂O₃, Er₂O₃, Y₂O₃, Ho₂O₃, Dy₂O₃, Tb₂O₃, Gd_2O_3 , Eu_2O_3 , Sm_2O_3 , Nd_2O_3 , Pr_2O_3 , CeO_2 , La_2O_3 , and Al_2O_3 of at least 99.99% purity. The powders were dried at 800 °C for 8 h in air, mixed in stoichiometric ratios, and placed in a Ø 16 mm iridium crucible with a Ø3 mm die and a Ø 0.5 mm capillary channel. The crucible was inductively heated to melt the powders, and two types of seed material were used to initiate the growth. An orthorhombic YAlO₃ seed oriented in the [001] direction was used for crystals A, B, C, D, and F. An orthorhombic structure was expected for those crystals since most of the constituent REs form an orthorhombic single-RE REAlO₃ (Table 2). An iridium pin was used for crystals E and G. A rhombohedral structure was expected for those crystals since most of the constituent REs form a rhombohedral single-RE REAlO₃ (Table 2); however, a rhombohedral crystal seed was not available. All crystals were grown with a pulling rate of 0.05 mm/min. Details about the mPD growth method and the crystal growth setup used here can be found in a previous publication.

2.3. Powder X-ray Diffraction. All crystals were subjected to phase analysis by acquiring room-temperature powder X-ray diffraction (XRD) patterns, which were used for Rietveld structure refinement. Crystals were cut into three cylindrical sections of equal lengths, and the middle section was ground in a mortar and used for phase analysis. Diffraction patterns were collected with a Panalytical Empyrean diffractometer in the Bragg–Brentano geometry using a Cu $K\alpha$ X-ray source at 45 kV and 40 mA. Lattice parameter and phase composition were obtained via Rietveld refinements with the General Structure Analysis System II software (GSASII). In the refinements, the fractional site occupancy of the five distinct REs was set to 1/5 in the RE crystallographic sites.

2.4. Single Crystal X-ray Diffraction. Crystals that were phase pure according to powder XRD results were subjected to single crystal XRD for further assessment of the crystal structure. A Rigaku XtaLAB PRO diffractometer equipped with a Rigaku HyPix-6000HE detector and an Oxford N-HeliX cryocooler was used to collect single-crystal diffraction data at room temperature. Graphite monochromated Mo K α radiation was used (λ = 0.71073 Å, 50 kV, and 40 mA). Peak indexing and integration were performed using the Rigaku Oxford Diffraction CrysAlisPro software.³⁹ An empirical absorption correc-

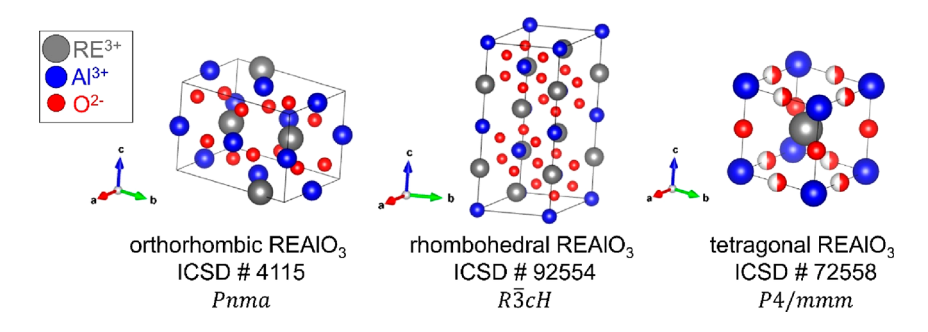


Figure 1. Schematic representation of the REAlO₃ unit cells with an orthorhombic (left), rhombohedral (center), and tetragonal structure (right). Images were generated with VESTA (Visualization for Electronic and STructural Analysis) using the CIF (Crystallographic Information File) obtained from ICSD (Inorganic Crystal Structure Database). The ICSD CIF numbers are provided in the image.

Table 2. List of Compositions and the Respective Number of REs That Form Each of the Four Structures Seen in Single-RE REAlO₃^a

			Number of R structures o			
ID	Composition	REs with consecutive ionic radius values in Table1?	O (Pnma)	$R(R\overline{3}c)$	T (P4/mmm)	AIR (Å)
A	(Yb,Tm,Er,Y,Ho)AlO ₃	Yes	5	0	0	0.879
В	(Y,Ho,Dy,Tb,Gd)AlO ₃	Yes	5	0	0	0.911
C	(Lu,Er,Y,Gd,Sm)AlO ₃	No	5	0	0	0.905
D	(Dy,Tb,Gd,Eu,Sm)AlO ₃	Yes	5	0	0	0.937
E	(Sm,Nd,Pr,Ce,La)AlO ₃	Yes	1	3	1	1.013
F	(Lu,Yb,Y,Gd,La)AlO ₃	No	4	1	0	0.919
G	(Lu,Nd,Pr,Ce,La)AlO ₃	No	1	3	1	0.990

^aO – orthorhombic, R – rhombohedral, T – tetragonal. Crystallographic space groups are in parentheses. Commas in the compositions represent equiatomic amounts of REs. Average ionic radii (AIR) for coordination number VI are listed.³⁷

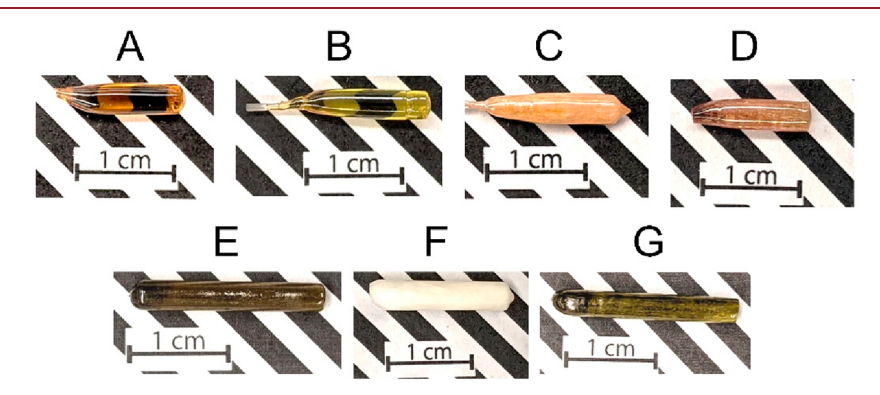


Figure 2. Cylindrical Ø3 mm crystals. Crystal IDs A-G corresponds to the compositions listed in Table 2. Crystals A, B, and D are translucent and crystals C, E, F, and G are opaque. The seed- and the tail-end of the crystals are on the left and right sides of the photos, respectively. A piece of the YAlO₃ seed is seen on the seed-end of crystal B.

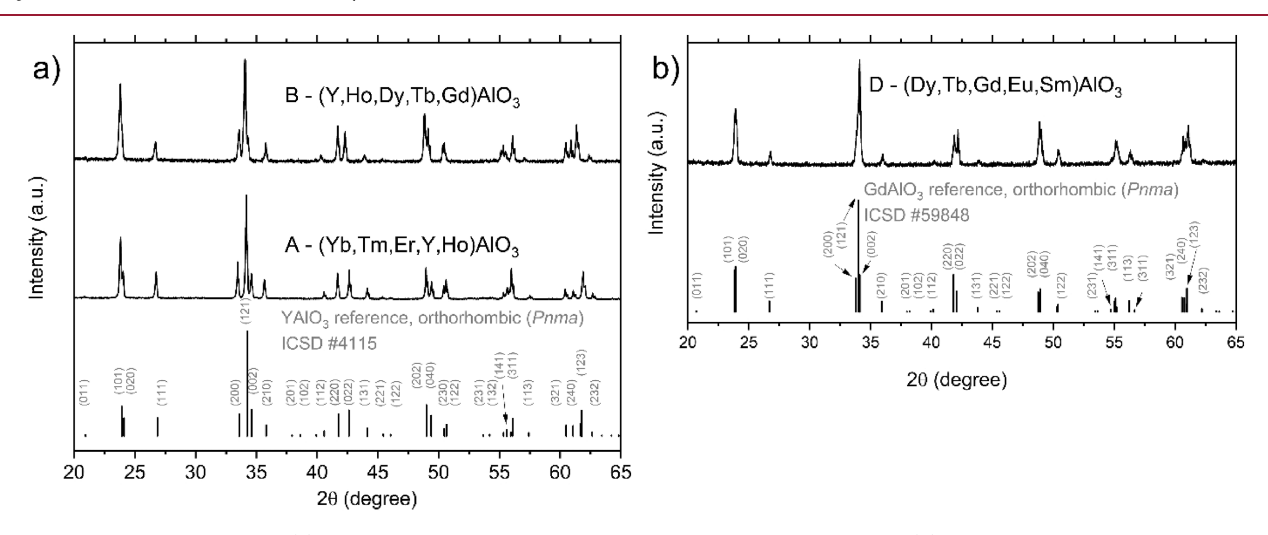


Figure 3. Powder XRD patterns of (a) crystals A and B and an orthorhombic YAlO₃ reference pattern; (b) crystal D and an orthorhombic GdAlO₃ reference pattern. The ICSD reference numbers are listed in the figures.

tion was applied using the SCALE3 ABSPACK algorithm as implemented in CrysAlisPro. The SHELXL-2013 and WinGX software packages were used for data processing and structure refinement. The structure refinements were made with oxygen atom positional coordinates, isotropic atomic displacement parameters, an extinction parameter, and the scale factor. In the refinements, the fractional site occupancy of the five distinct REs was set to 1/5 in the RE crystallographic sites.

2.5. Scanning Electron Microscopy and Energy Dispersive Spectroscopy. To evaluate the microstructure of the crystals, 1 mm thick cross-sectional samples were cut, polished, and imaged with a Zeiss EVO MA15 Scanning Electron Microscope (SEM). The

elemental composition of the samples was analyzed with a Bruker xFlash 6130 Energy Dispersive X-ray Spectrometer (EDS), which was mounted in the SEM sample chamber.

3. RESULTS AND DISCUSSION

3.1. Grown Crystals. Crystals containing only REs with consecutive ionic radius values and that form orthorhombic single-RE REAlO₃ (crystals A, B, and D) are translucent. As seen in Figure 2, crystals A and B are crack-free and translucent, while crystal D is heavily cracked with a translucent section on the seed-end (left side of the photo).

Crystal D was translucent during growth and cracked upon cooling, which is a common issue in orthorhombic REAlO₃ crystals due to their anisotropic coefficients of thermal expansion. Cracking in composition D may be avoided by growing crystals with a longer neck and shoulder section to prevent seed defects from propagating into the crystal. The translucency in these crystals is related to a phase-pure structure as discussed in the next section. The orange color in those crystals comes from Ho³⁺, Dy³⁺, and Sm³⁺.

Crystals that contain REs with nonconsecutive ionic radius values or mixtures of REs that form an orthorhombic, rhombohedral, and tetragonal single-RE REAlO $_3$ are opaque (crystals C, E, F, and G). These crystals were opaque during growth and at room temperature, which may indicate polycrystallinity due to a mixture of phases as discussed in the next section. Crystal C is orange due to Sm $^{3+}$, while crystals E and G are dark green due to Pr $^{3+}$.

3.2. Phase Formation and Crystal Structure. 3.2.1. Powder XRD. Crystals A, B, and D are a single orthorhombic phase, which may have been favored by mixtures of REs that have similar ionic radii and form orthorhombic single-RE REAlO₃ (Table 2). Powder XRD patterns of crystals A and B have reflection peaks that match those of an orthorhombic YAlO₃ reference pattern as seen in Figure 3a. A powder XRD pattern is shown in Figure 3b and indicates that the reflection peaks of crystal D match those of an orthorhombic GdAlO₃ reference pattern. These reference patterns were chosen due to the similarity of their RE³⁺ ionic radius and the AIR of compositions A, B, and D (Table 1 and Table 2).

The lattice parameters of crystals A, B, and D follow the general trend of single-RE REAlO₃ with respect to the RE³⁺ average ionic radius, as seen in Figure 4. In general, with an increasing RE³⁺ ionic radius, the unit cell volume of single-RE REAlO₃ increases with the b and c axes while the a axis decreases. The perovskites formed by Er³⁺, Y³⁺, and Dy³⁺ are exceptions, and their a axes are larger than the ones of the perovskites formed by the immediately preceding REs in Figure 4. Nevertheless, the general trend is also observed for

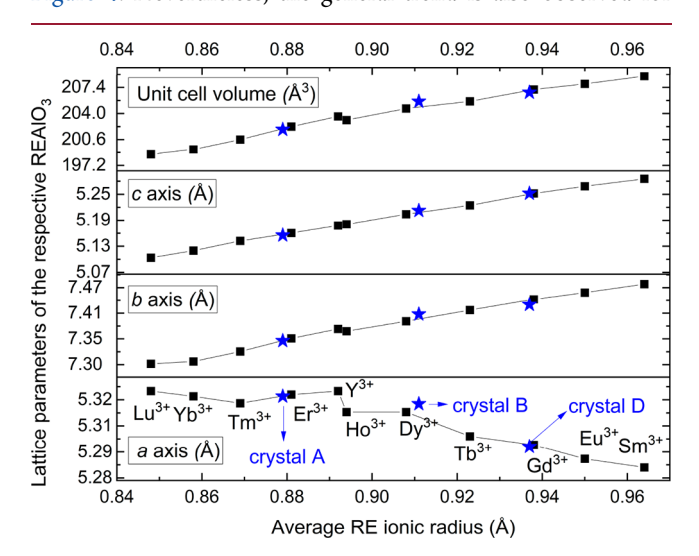


Figure 4. Lattice parameters of orthorhombic single-RE REAlO $_3$ (squares) from the literature 27,42 and those of the high entropy crystals A, B, and D (stars) obtained via powder XRD data and Rietveld refinement (Table 3). The labels in the bottom graph apply to all graphs.

the high-entropy crystals A, B, and D. Additionally, the lattice parameters of crystals A, B, and D are similar to those of ErAlO₃, DyAlO₃, and GdAlO₃, respectively. Trivalent Er, Dy³⁺, and Gd³⁺ have ionic radius values close to the AIR of A, B, and D, respectively. This indicates that lattice parameters of high-entropy perovskites vary consistently with their AIR.

The successful growth of crystals A, B, and D demonstrates the practical aspect of growing phase-pure high-entropy REAlO₃ crystals. These crystals contain REs with consecutive ionic radius values as listed in Table 1; additionally, all constituent REs form orthorhombic single-RE REAlO₃. In the next paragraphs, we discuss how phase formation is affected by mixing REs that have nonconsecutive ionic radii or that form single-RE REAlO₃ with an orthorhombic, rhombohedral, and tetragonal structure.

Crystal C is a mixture of two orthorhombic structures, and the weight fraction of the primary and secondary phases are 90 and 10 wt % respectively; this mixture may have been induced by the dissimilarity in the ionic radius of the constituent REs. A powder XRD pattern of crystal C is shown in Figure 5.a with reference patterns of orthorhombic YAlO₃ and orthorhombic GdAlO₃. Similar to the single-phase crystals A, B, and D, crystal C only has REs that form orthorhombic single-RE REAlO₃. However, the single-phase crystals A, B, and D have REs with consecutive ionic radii values, while the REs in crystal C have nonconsecutive ionic radii values. Therefore, the formation of two orthorhombic phases may have resulted from the dissimilarity in the size of RE cations in crystal C. The unit cell volume of the primary and secondary orthorhombic unit cells are 202.724 $\text{Å}^{\frac{1}{3}}$ and 209.274 Å^{3} , which indicates that the larger REs such as Gd³⁺ and Sm³⁺ are concentrated in the secondary phase. Therefore, the REs in composition C are not homogeneously distributed between the primary and secondary orthorhombic phases.

Crystals E is a mixture of rhombohedral (86 wt %) and tetragonal (14 wt %) phases although the constituent REs have consecutive ionic radius values; this mixture may have resulted from combinations of REs that form orthorhombic, rhombohedral, or tetragonal single-RE REAlO₃ (Table 2). A powder XRD pattern of crystal E is shown in Figure 5b with reference patterns of rhombohedral NdAlO₃ and tetragonal CeAlO₃. Most of the REs in crystal E form rhombohedral single-RE REAlO₃ (Table 2), which explains a larger weight fraction of the rhombohedral phase. Therefore, it is likely that the RE elements are not homogeneously distributed between the two phases in crystal E and the rhombohedral phase may be richer in the REs that form rhombohedral single-RE perovskites (Nd, Pr, and La). Since no orthorhombic phases were observed, Sm3+ was likely incorporated in the rhombohedral or tetragonal phases, although SmAlO₃ is orthorhombic (Table 1). The AIR of composition E is close to the ionic radius of Pr^{3+} and $PrAlO_3$ is rhombohedral (Table 1 and Table 2). Therefore, the AIR of E may have favored the formation of a primary rhombohedral structure.

Crystal F is a mixture of a primary orthorhombic (45 wt %), a secondary orthorhombic (38 wt %), and rhombohedral (17 wt %) structures, which may have resulted from a mixture of REs that form different structures in single-RE REAlO₃ (Table 2). A powder XRD pattern of crystal F is shown in Figure 5c with reference patterns of orthorhombic YAlO₃, orthorhombic GdAlO₃, and rhombohedral NdAlO₃. Four of the five REs in composition F form orthorhombic single-RE REAlO₃, which explains the larger weight fraction of orthorhombic phases. As

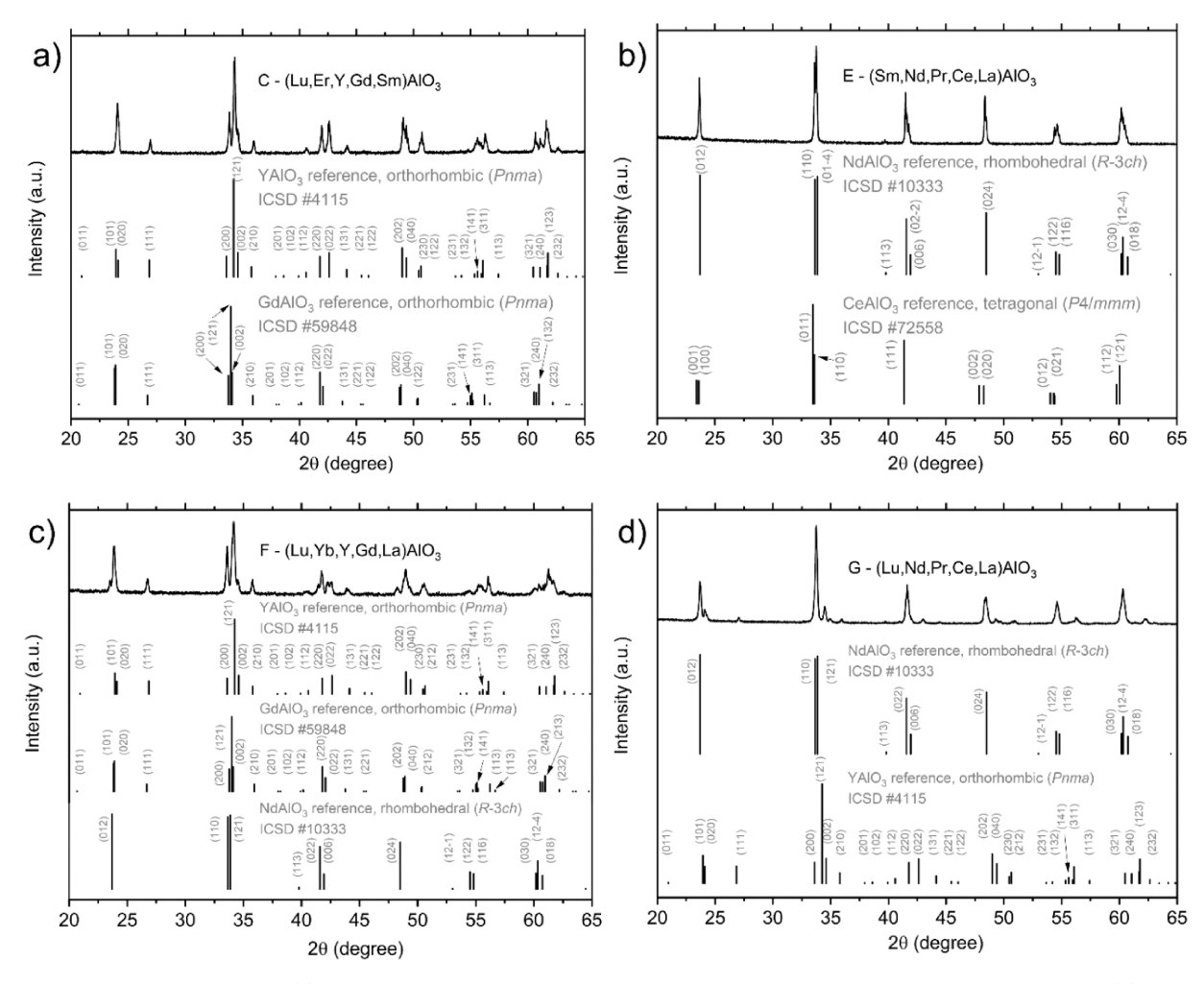


Figure 5. Powder XRD patterns of (a) crystal C, an orthorhombic YAlO₃, and an orthorhombic GdAlO₃ reference patterns; (b) crystal E, a rhombohedral NdAlO₃, and a tetragonal NdAlO₃ reference patterns; (c) crystal F, an orthorhombic YAlO₃, an orthorhombic GdAlO₃, and a rhombohedral NdAlO₃ reference patterns; (d) crystal G, a rhombohedral NdAlO₃, and an orthorhombic YAlO₃ reference patterns.

a result, having four REs that form the same structure in single-RE REAlO $_3$ and only one RE that forms a different structure is enough to induce a mixture of phases. The AIR of composition F is close to the ionic radius of Tb^{3+} and TbAlO_3 is orthorhombic. Therefore, the AIR of F may have favored the formation of the dominant orthorhombic structures.

Crystal G is a mixture of orthorhombic (39 wt %) and rhombohedral (61 wt %) structures, which may also have resulted from a mixture of REs that form different structures in single-RE REAlO₃ (Table 2). A powder XRD pattern of crystal G is shown in Figure 5d with reference patterns of orthorhombic YAlO₃ and rhombohedral NdAlO₃. Three of the five REs in composition G form rhombohedral single-RE REAlO₃, which explains the larger weight fraction of the rhombohedral phase. The AIR of composition F is close to the ionic radius of Nd³⁺ and NdAlO₃ is rhombohedral. Therefore, the AIR of G may have favored the formation of the dominant phase.

The high-entropy nature of crystals C, E, F, and G does not stabilize a single phase and the structures formed depend on the type of REs in each composition. Combinations of REs with dissimilar ionic radius values and combinations of REs that form an orthorhombic, rhombohedral, and tetragonal single-RE REAlO₃ hinder the formation of single-phases.

Therefore, such combinations should be avoided to design phase-pure high-entropy REAlO₃ crystals.

3.2.2. Single Crystal XRD. Single crystal XRD results confirm a single orthorhombic Pnma structure in crystals A and B. These two crystals were selected for further structural investigation because they were a single phase according to powder XRD and did not crack during the growth. The RE site occupation was held fixed at the nominal composition since the number of elements on the RE site makes site occupation refinements underdetermined. No short-range clustering of the REs was observed since the diffraction patterns indicated no obvious diffuse scattering. The refinement parameters from single-crystal X-ray diffraction are given in the Supporting Information in Table S1. Fractional atomic coordinates and isotropic displacement parameters are listed in Table S2. The refined lattice parameters are like those obtained via refinement from powder XRD data in Table 3. Therefore, single crystal XRD data confirms a smaller unit cell volume for crystal A compared to B, although the lattice parameter a of crystal A is slightly larger than that of B.

3.3. Radial Elemental Distribution in Single-Phase Crystals. According to EPMA radial concentration profiles, there is no clear evidence of preferential incorporation of any REs in crystals A and B. In general, mPD crystals are compositionally homogeneous along the growth axis, elemental

Table 3. Lattice Parameters and Phase Fraction of Crystals A–F Obtained via Rietveld Structure Refinement Using Powder XRD Data^a

				Refine	ed unit ce	Il lattice param	teters (a, b, an)	d c in Å) and	phase fra	ction (PF in v	Refined unit cell lattice parameters $(a,b,$ and c in $Å$) and phase fraction (PF in wt $\%$) of each structure	tructure			
		0	Orthorhombic PP (Pnma)	PP (Pnma)		0	Orthorhombic SP (Pnma)	P (Pnma)		[Rhom]	Rhombohedral $(R\overline{3}c)$		Tetrago	Tetragonal $(P4/mmm)$	
Sample ID	Composition	а	9	2	PF	а	9	2	PF	а	2	PF	а	2	PF
A	(Yb,Tm,Er,Y,Ho)AlO ₃	5.327(0)	7.348(9)	5.157(8)	100			1	,			,	,	·	,
В	$(Y,Ho,Dy,Tb,Gd)AIO_3$	5.322(6)	7.407(4)	5.214(0)	100			ı	,	1		,		ı	,
С	$(Lu,Er,Y,Gd,Sm)AIO_3$	5.301(9)	7.375(3)	5.184(3)	06	5.299(9)	7.463(5)	5.290(7)	10	1		,		ı	,
О	$(Dy,Tb,Gd,Eu,Sm)AIO_3$	5.298(0)	7.428(8)	5.253(0)	100		,	ı	,		1	,		ı	,
Э	(Sm,Nd,Pr,Ce,La)AlO ₃	1	1	1		1	1	ı	,	5.332(2)	12.963(4)	98	3.753(7)	3.761(3)	14
ц	$(Lu, Yb, Y, Gd, La)AIO_3$	5.322(3)	7.378(2)	5.180(2)	45	5.315(5)	7.409(7)	5.220(9)	38	5.331(5)	12.992(1)	17	1	ı	,
Ŋ	$(Lu,Nd,Pr,Ce,La)AIO_3$	5.327(3)	7.336(8)	5.141(9)	39	1			,	5.327(2)	13.016(3)	61			1
^a The acron	^a The acronyms PP and SP stand for "primary phase" and "secondary phase", respectively.	primary phas	e" and "secon	ndary phase",	respect	ively.									

segregation, and preferential incorporation may be seen in cross-sectional elemental distribution profiles. 1,38 Radial concentration profiles of crystals A and B are seen in Figure 6a and b; the nominal concentration of each RE is 4 at%. These crystals were selected for elemental distribution studies because they are phase pure and not cracked. In crystal A, the elemental profiles are close to nominal concentration and close to horizontal from -1.1 to 1.1 mm. Discontinuities close to the outer edge of the crystal (-1.5 to -1.2 mm and 1.2 to 1.5mm) may result from better mixing of the melt achieved by the Marangoni melt flow that occurs close to the outer surface of the melt in the molten zone. In crystal B, the distribution profiles are close to horizontal along the whole diameter of the crystal. Since the elemental distribution profiles are close to horizontal along most of the crystal diameter, none of the RE species is preferentially incorporated into the crystals. This is in contrast with previously published high-entropy aluminum garnet mPD crystals (RE₃Al₅O₁₂) in which the preferential incorporation of smaller REs was evident by significantly curved profiles. 1,7

3.4. Distribution and Composition of Secondary Phases. Crystal G (Lu,Nd,Pr,Ce,La)AlO₃ has a Lu-rich secondary phase in a matrix with a composition that is closer to the nominal stoichiometry. Crystal G is the focus of this section since its SEM images have more phase separation features than the other crystals with multiple phases (crystals C, E, and F; Table 3). An SEM image of a cross-sectional sample is seen in Figure 7a and reveals a lighter area in the center with branching structures closer to the outer surface of the crystal. To assess the elemental composition of both the lighter areas and the darker matrix, EDS data were collected from the six points shown in Figure 7b and are presented in Table 4. The lighter areas (points 1-3) are Lu-rich and are likely to have the orthorhombic structure that is typical of LuAlO₃ (Table 1) and was observed in crystal G (Table 3). The darker matrix (points 4-6) has a composition that is closer to stoichiometric but is also slightly rich in Lu; the matrix is likely to have the primary rhombohedral phase observed in crystal F (Table 3). Although Al-rich inclusions have been previously reported for LaAlO₃ mPD crystals; 43 here the general ratio of RE to Al concentrations is close to stoichiometric for all points assessed. This indicates no significant deviation from the nominal REAlO3 perovskite stoichiometry.

4. CONCLUSION

High-entropy REAlO₃ single crystals can be grown via directional solidification, and phase formation depends on the composition. Here we reported the practical aspect of growing five-component equiatomic REAlO₃ via the micropulling-down method and determined the effects of composition on phase formation. Crystals containing only REs with similar ionic radii and that form orthorhombic single-RE REAlO₃ are a single orthorhombic phase. On the other hand, crystals containing a combination of REs with dissimilar ionic radii or that form an orthorhombic, rhombohedral, and tetragonal single-RE REAlO₃ are a mixture of phases. In single crystal samples, there is no evidence of preferential incorporation of any of the REs into the crystal. In multiphase crystals, the secondary phase is concentrated in the center of the crystal with a branching structure closer to the outer edge.

Demonstrations of the crystal growth of high-entropy oxides encourage the exploration of potential functional properties in

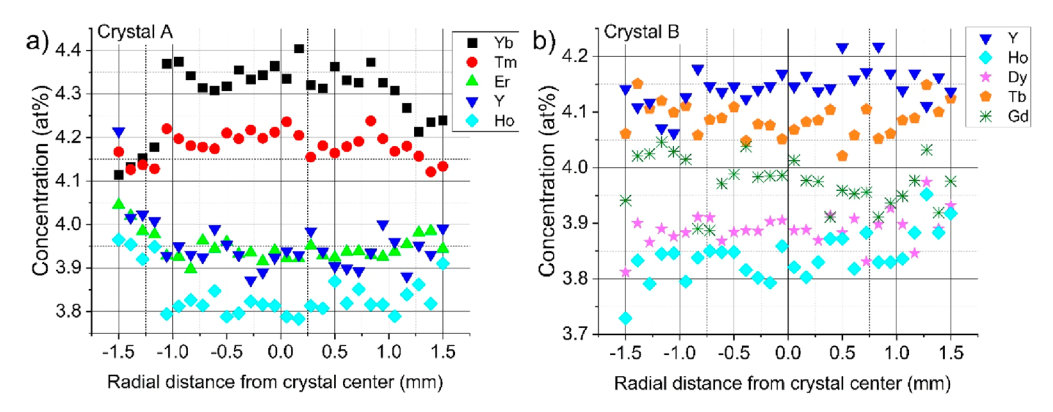


Figure 6. Radial concentration profiles obtained with EPMA for crystals (a) A (Yb,Tm,Er,Y,Ho)AlO₃ and (b) B (Y,Ho,Dy,Tb,Gd)AlO₃. The nominal concentration of each RE is 4 at%.

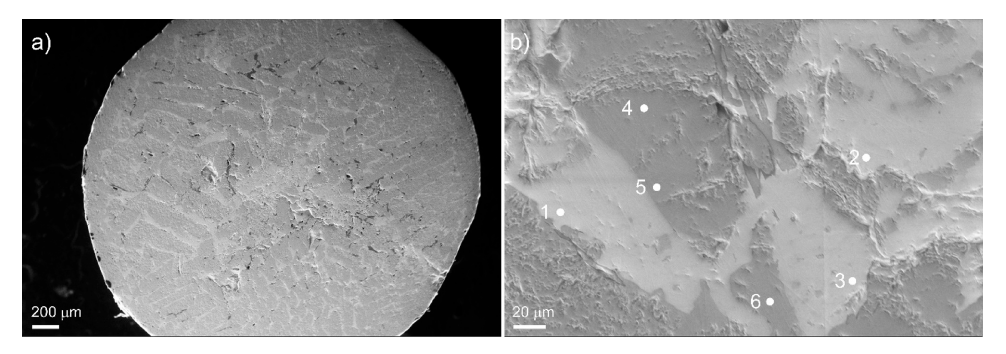


Figure 7. SEM images of a cross-sectional sample from crystal G (Lu,Nd,Pr,Ce,La)AlO₃ using low (a) and high (b) magnification. The elemental composition was analyzed via EDS for the points identified with numbers in (b); EDS results are presented in Table 4.

Table 4. Elemental Composition of Crystal F (Lu,Nd,Pr,Ce,La)AlO₃ for Areas 1-6 Shown in the SEM Image in Figure 7b

					EDS ele	emental com	position (at%), error <0.00	1 at%
Area	Points from Figure 6b	Lu	Nd	Pr	Ce	La	Al	O	Stoichiometry
	Nominal composition	4	4	4	4	4	20	60	$RE_1Al_1O_3$
Lighter area	1	20.2	2.1	2.4	2.6	2.6	31.4	38.7	$RE_{1.0}Al_{1.1}O_{1.3}$
	2	20.1	1.7	1.9	2.0	1.8	33.9	38.6	$RE_{1.0}Al_{1.2}O_{1.4}$
	3	20.1	1.9	2.1	2.2	2.3	33.0	38.4	$RE_{1.0}Al_{1.2}O_{1.3}$
Darker area	4	6.5	4.4	5.5	6.2	4.2	33.7	39.5	$RE_{1.0}Al_{1.3}O_{1.5}$
	5	6.1	4.5	5.3	6.1	6.4	32.7	38.9	$RE_{1.0}Al_{1.2}O_{1.4}$
	6	6.9	4.3	5.0	5.8	6.0	32.6	39.4	$RE_{1.0}Al_{1.2}O_{1.4}$

highly complex single crystals, including luminescence and magnetic properties. The findings reported here may be leveraged for future studies on compositionally complex perovskite crystals. High-entropy versions of the traditional host crystals YAlO₃ and LuAlO₃ may reveal attractive luminescence properties for scintillation and lasing applications. To develop such materials, future efforts should focus on compositions containing only REs with similar ionic radii and that form orthorhombic single-RE REAlO₃ so that single-phase crystals can be produced with high optical quality. Additionally, future investigation could focus on admixing Ga³⁺ into the Al³⁺ sites to determine whether structural and functional properties can be optimized.

ASSOCIATED CONTENT

Supporting Information

The Supporting Information is available free of charge at https://pubs.acs.org/doi/10.1021/acs.cgd.2c01130.

Single-crystal X-ray diffraction data collection, refinement parameters, fractional atomic coordinates, and equivalent isotropic displacement parameters for crystals A (Yb,Tm,Er,Y,Ho)AlO₃ and B (Y,Ho,Dy,Tb,Gd)AlO₃ (PDF)

Accession Codes

CCDC 2215916–2215917 contain the supplementary crystallographic data for this paper. These data can be obtained free of charge via www.ccdc.cam.ac.uk/data_request/cif, or by emailing data_request/cif, or by contacting The Cambridge Crystallographic Data Centre, 12 Union Road, Cambridge CB2 1EZ, UK; fax: +44 1223 336033.

AUTHOR INFORMATION

Corresponding Author

Matheus Pianassola — Scintillation Materials Research Center, University of Tennessee, Knoxville, Tennessee 37996, United States; Department of Materials Science and Engineering, University of Tennessee, Knoxville, Tennessee 37996, United States; orcid.org/0000-0001-7468-2794; Email: mpianass@vols.utk.edu

Authors

Bryan C. Chakoumakos – Neutron Scattering Division, Oak Ridge National Laboratory, Oak Ridge, Tennessee 37831, United States

Charles L. Melcher — Scintillation Materials Research Center, University of Tennessee, Knoxville, Tennessee 37996, United States; Department of Materials Science and Engineering, University of Tennessee, Knoxville, Tennessee 37996, United States; Department of Nuclear Engineering, University of Tennessee, Knoxville, Tennessee 37996, United States

Mariya Zhuravleva — Scintillation Materials Research Center, University of Tennessee, Knoxville, Tennessee 37996, United States; Department of Materials Science and Engineering, University of Tennessee, Knoxville, Tennessee 37996, United States

Complete contact information is available at: https://pubs.acs.org/10.1021/acs.cgd.2c01130

Notes

The authors declare no competing financial interest.

ACKNOWLEDGMENTS

This work was supported by the National Science Foundation (DMR 1846935). Powder XRD was performed at the Institute for Advanced Materials & Manufacturing (IAMM) Diffraction Facility, located at the University of Tennessee, Knoxville. Electron microprobe measurements were performed at the Electron Microprobe Laboratory in the Department of Earth and Planetary Sciences at the University of Tennessee, Knoxville with the assistance of Molly McCanta and Allan Patchen. A portion of this research used resources at the Spallation Neutron Source, a Department of Energy Office of Science User Facility operated by the Oak Ridge National Laboratory.

REFERENCES

- (1) Pianassola, M.; Loveday, M.; Chakoumakos, B. C.; Koschan, M.; Melcher, C. L.; Zhuravleva, M. Crystal Growth and Elemental Homogeneity of the Multicomponent Rare-Earth Garnet (Lu1/6Y1/6Ho1/6Dy1/6Tb1/6Gd1/6)3Al5O12. Cryst. Growth Des. 2020, 20 (10), 6769–6776.
- (2) Kinsler-Fedon, C.; Zheng, Q.; Huang, Q.; Choi, E. S.; Yan, J.; Zhou, H.; Mandrus, D.; Keppens, V. Synthesis, Characterization, and Single-Crystal Growth of a High-Entropy Rare-Earth Pyrochlore Oxide. *Phys. Rev. Mater.* **2020**, *4* (10), 104411.
- (3) Gheorghe, L.; Khaled, F.; Achim, A.; Voicu, F.; Loiseau, P.; Aka, G. Czochralski Growth and Characterization of Incongruent Melting LaxGdyScz(BO3)4 (x + y + z = 4) Nonlinear Optical Crystal. *Cryst. Growth Des.* **2016**, *16* (6), 3473–3479.
- (4) Rost, C. M.; Sachet, E.; Borman, T.; Moballegh, A.; Dickey, E. C.; Hou, D.; Jones, J. L.; Curtarolo, S.; Maria, J.-P. P. Entropy-Stabilized Oxides. 2015, 6 (1), 1–8.
- (5) Musicó, B. L.; Gilbert, D.; Ward, T. Z.; Page, K.; George, E.; Yan, J.; Mandrus, D.; Keppens, V. The Emergent Field of High Entropy Oxides: Design, Prospects, Challenges, and Opportunities for Tailoring Material Properties. *APL Mater.* **2020**, *8* (4), 040912.
- (6) Pianassola, M.; Stand, L.; Loveday, M.; Chakoumakos, B. C.; Koschan, M.; Melcher, C. L.; Zhuravleva, M. Czochralski Growth and Characterization of the Multicomponent Garnet (Lu1/4Yb1/4Y1/4Gd1/4)3Al5O12. *Phys. Rev. Mater.* **2021**, *5* (8), 083401.
- (7) Pianassola, M.; Alexander, M.; Chakoumakos, B.; Koschan, M.; Melcher, C.; Zhuravleva, M. Effects of Composition and Growth

- Parameters on Phase Formation in Multicomponent Aluminum Garnet Crystals. *Acta Crystallogr. B. Struct. Sci. Cryst. Eng. Mater.* **2022**, 78, 476–484.
- (8) Kinsler-Fedon, C.; Nuckols, L.; Nelson, C. T.; Qi, Z.; Huang, Q.; Mandrus, D.; Zhang, Y.; Weber, W. J.; Keppens, V. Effects of Au2+Irradiation Induced Damage in a High-Entropy Pyrochlore Oxide Single Crystal. *Scr. Mater.* **2022**, 220, 114916.
- (9) Greculeasa, M.; Broasca, A.; Voicu, F.; Hau, S.; Croitoru, G.; Stanciu, G.; Gheorghe, C.; Pavel, N.; Gheorghe, L. Bifunctional LaxNdyGdzSc4-x-y-z(BO3)4 Crystal: Czochralski Growth, Linear and Nonlinear Optical Properties, and near-Infrared Laser Emission Performances. *Opt. Laser Technol.* **2020**, *131*, 106433.
- (10) Liu, F.; Dong, L.; Cao, S.; Chen, J.; Xu, H.; Han, W.; Liu, J. Crystal Growth, Structural Characterization and Laser Operation of an Yb0.19Y0.34Lu0.12Gd0.35Ca4O(BO3)3 Mixed Crystal. *J. Cryst. Growth* 2021, 558, 126023.
- (11) Han, W.; Dong, L.; Zhou, Y.; Zhang, Y.; Xu, H.; Liu, J. Spectroscopic Properties and Laser Emission of Yb0.05Y0.20La0.12Gd0.63Ca4O(BO3)3 Mixed Oxyborate Crystal. Laser Phys. Lett. 2022, 19 (5), 055802.
- (12) Kränkel, C.; Uvarova, A.; Haurat, É.; Hülshoff, L.; Brützam, M.; Guguschev, C.; Kalusniak, S.; Klimm, D. IUCr. Czochralski Growth of Mixed Cubic Sesquioxide Crystals in the Ternary System Lu2O3—Sc2O3—Y2O3. *Acta Crystallogr.* **2021**, *77* (4), 550—558.
- (13) Nikl, M.; Yoshikawa, A.; Kamada, K.; Nejezchleb, K.; Stanek, C. R.; Mares, J. A.; Blazek, K. Development of LuAG-Based Scintillator Crystals A Review. *Prog. Cryst. Growth Charact. Mater.* **2013**, 59 (2), 47–72.
- (14) Ikesue, A.; Aung, Y. L.; Taira, T.; Kamimura, T.; Yoshida, K.; Messing, G. L. Progress in Ceramic Lasers. *Annu. Rev. Mater. Res.* **2006**, 36 (3), 397–429.
- (15) Nikl, M.; Yoshikawa, A. Recent R&D Trends in Inorganic Single-Crystal Scintillator Materials for Radiation Detection. *Adv. Opt. Mater.* **2015**, 3 (4), 463–481.
- (16) Elder, I. F.; Payne, M. J. P. YAP versus YAG as a Diode-Pumped Host for Thulium. *Opt. Commun.* **1998**, *148* (4–6), 265–269.
- (17) Kamada, K.; Endo, T.; Tsutumi, K.; Yanagida, T.; Fujimoto, Y.; Fukabori, A.; Yoshikawa, A.; Pejchal, J.; Nikl, M. Composition Engineering in Cerium-Doped (Lu,Gd)3(Ga,Al) 5O12 Single-Crystal Scintillators. *Cryst. Growth Des.* **2011**, *11* (10), 4484–4490.
- (18) Kamada, K.; Yanagida, T.; Pejchal, J.; Nikl, M.; Endo, T.; Tsutumi, K.; Fujimoto, Y.; Fukabori, A.; Yoshikawa, A. Scintillator-Oriented Combinatorial Search in Ce-Doped (Y,Gd) 3(Ga,Al) 5O 12 Multicomponent Garnet Compounds. J. Phys. D. Appl. Phys. 2011, 44 (50), 505104–505112.
- (19) Chewpraditkul, W.; Pánek, D.; Brůža, P.; Chewpraditkul, W.; Wanarak, C.; Pattanaboonmee, N.; Babin, V.; Bartosiewicz, K.; Kamada, K.; Yoshikawa, A.; Nikl, M. Luminescence Properties and Scintillation Response in Ce3+-Doped Y2Gd1Al5-XGaxO12 (x = 2, 3, 4) Single Crystals. *J. Appl. Phys.* **2014**, *116* (8), 083505.
- (20) Sakthong, O.; Chewpraditkul, W.; Chewpraditkul, W.; Kurosawa, S.; Yoshikawa, A.; Kamada, K.; Kim, K. J.; Drozdowski, W.; Witkowski, M. E.; Makowski, M.; Kucerkova, R.; Beitlerova, A.; Nikl, M. Luminescence and Scintillation Properties of Mo Co-Doped Y0.8Gd2.2(Al5-XGax)O12: Ce Multicomponent Garnet Crystals. Opt. Mater. (Amst). 2021, 122, 111783.
- (21) Garton, G.; Wanklyn, B. M. The Rare Earth Aluminates. J. Cryst. Growth 1967, 1 (3), 164–166.
- (22) Pokorný, M.; Babin, V.; Beitlerová, A.; Jurek, K.; Polák, J.; Houžvička, J.; Pánek, D.; Parkman, T.; Vaněček, V.; Nikl, M. Gd-Admixed (Lu,Gd)AlO3 Single Crystals: Breakthrough in Heavy Perovskite Scintillators. NPG Asia Mater. 2021, 13 (1), 1–9.
- (23) Gieszczyk, W.; Bilski, P.; Klosowski, M.; Mrozik, A.; Zorenko, Y.; Zorenko, T.; Paprocki, K. Luminescent Properties of Undoped and Ce3+ Doped Crystals in Y2O3 Lu2O3 Al2O3 Triple Oxide System Grown by Micro-Pulling-down Method. *Opt. Mater.* (Amst). 2019, 89, 408–413.

- (24) Gieszczyk, W.; Bilski, P.; Kłosowski, M.; Mrozik, A.; Zorenko, T.; Witkiewicz, S.; Zorenko, Y. Luminescent Properties of Tb and Eu Activated AxB1-XAlO3 (A = Y, Lu, Gd; B = Lu; x = 0, 0.5, 1) Mixed Oxides Crystals Prepared by Micro-Pulling-down Method. *Radiat. Meas.* 2019, 126, 106140.
- (25) Horiai, T.; Pejchal, J.; Paterek, J.; Kucerkova, R.; Yokota, Y.; Yoshikawa, A.; Nikl, M. Crystal Growth and Optical Properties of CeDoped (Y, Lu)AlO3 Single Crystal. *Jpn. J. Appl. Phys.* **2022**, *61* (7), 072002.
- (26) Zhao, Z.; Chen, H.; Xiang, H.; Dai, F. Z.; Wang, X.; Xu, W.; Sun, K.; Peng, Z.; Zhou, Y. High-Entropy (Y0.2Nd0.2Sm0.2Eu0.2Er0.2)AlO3: A Promising Thermal/Environmental Barrier Material for Oxide/Oxide Composites. *J. Mater. Sci. Technol.* 2020, 47, 45–51.
- (27) Shishido, T.; Nojima, S.; Tanaka, M.; Horiuchi, H.; Fukuda, T. Flux Growth of Perovskite-Type RAIO3 Single Crystals. *J. Alloys Compd.* **1995**, 227 (2), 175–179.
- (28) Diehl, R.; Brandt, G. Crystal Structure Refinement of YAlO3, a Promising Laser Material. *Mater. Res. Bull.* **1975**, *10* (2), 85–90.
- (29) Mizuno, M. Phase Diagrams of the Systems Al2O3-Ho2O3 and Al2O3-Er2O3 at High Temperatures. *Yogyo Kyokaishi* **1979**, 87 (1008), 405–412.
- (30) Holmes, L.; Sherwood, R.; Van Uitert, L. G. Metamagnetism in TbAlO3. *J. Appl. Phys.* **1968**, 39 (2), 1373.
- (31) Shilpa, C. J.; Jayaram, A. K.; Dhananjaya, N.; Nagabhushana, H.; Prashantha, S. C.; Sunitha, D. V.; Sharma, S. C.; Shivakumara, C.; Nagabhushana, B. M. GdAlO3:Eu3+:Bi3+ Nanophosphor: Synthesis and Enhancement of Red Emission for WLEDs. *Spectrochim. Acta Part A Mol. Biomol. Spectrosc.* **2014**, *133*, 550–558.
- (32) Sakhya, A. P.; Dutta, A.; Shannigrahi, S.; Sinha, T. Electronic Structure, Optical Dielectric Constant and Born Effective Charge of EuAlO3. *J. Phys. Chem. Solids* **2016**, 88, 1–7.
- (33) Geller, S.; Bala, V. B. Crystallographic Studies of Perovskite-like Compounds. II. Rare Earth Aluminates. *Acta Crystallogr.* **1956**, *9* (12), 1019–1025.
- (34) Brusset, H.; Gillier-Pandraud, M. H.; Saine, M. C. Sur Des Gallates et Aluminates Mixtes de Lanthanides. *Mater. Res. Bull.* **1975**, 10 (6), 481–488.
- (35) Tanaka, M.; Shishido, T.; Horiuchi, H.; Toyota, N.; Shindo, D.; Fukuda, T. Structure Studies of CeAlO3. *J. Alloys Compd.* **1993**, 192 (1–2), 87–89.
- (36) Tseng, K. P.; Yang, Q.; McCormack, S. J.; Kriven, W. M. High-Entropy, Phase-Constrained, Lanthanide Sesquioxide. *J. Am. Ceram. Soc.* **2020**, *103* (1), 569–576.
- (37) Shannon, R. D.; Prewitt, C. T. Effective Ionic Radii in Oxides and Fluorides. *Acta Crystallogr. Sect. B Struct. Crystallogr. Cryst. Chem.* **1969**, 25 (5), 925–946.
- (38) Fukuda, T.; Chani, V. I.; Fukuda, T.; Chani, V. I. Shaped Crystals: Growth by the Micro-Pulling-Down Technique. *Advances in Materials Research* **2007**, 1 DOI: 10.1007/978-3-540-71295-4.
- (39) Rigaku. CrystalClear; Rigaku Corporation: Tokyo, Japan, 2005.
- (40) Cockayne, B.; Lent, B.; Abell, J. S.; Harris, I. R. Cracking in Yttrium Orthoaluminate Single Crystals. *J. Mater. Sci.* **1973**, *8*, 871–875.
- (41) Lu, Y.; Wang, J.; Yang, Y.; Dai, Y.; Sun, B.; Li, S. Czochralski Growth of YAP Crystal Doped with High Tm Concentration. *J. Cryst. Growth* **2006**, 292 (2), 381–385.
- (42) Bondar, I. A.; Koroleva, L. N.; Bezruk, E. T. Physicochemical Properties of Yttrium Aluminates and Gallates. *Izv. Akad. Nauk SSSR, Neorg. Mater.* **1984**, 20 (2), 257–261.
- (43) Pejchal, J.; Babin, V.; Buryi, M.; Laguta, V.; Hájek, F.; Páterek, J.; Procházková-Prouzová, L.; Havlák, L.; Czerneková, V.; Vaněček, V.; Doležal, V.; Havlíček, J.; Rubešová, K.; Zemenová, P.; Falvey, A.; Král, R.; Pankratov, V.; Chernenko, K. Untangling the Controversy on Ce 3+ Luminescence in LaAlO 3 Crystals. *Mater. Adv.* **2022**, 3 (8), 3500–3512.